ChemPubSoc Europe

DOI: 10.1002/ejic.201901055

EurJIC European Journal of Inorganic Chemistry

Full Paper

Anticancer Complexes | *Very Important Paper* |

Ligand-Controlled Reactivity and Cytotoxicity of Cyclometalated Rhodium(III) Complexes

Wen-Ying Zhang,[a] Hannah E. Bridgewater,[a] Samya Banerjee,[a] Joan J. Soldevila-Barreda,[a] Guy J. Clarkson,[a] Huayun Shi,[a] Cinzia Imberti,[a] and Peter J. Sadler*[a]

Abstract: We report the synthesis, characterization and cytotoxicity of six cyclometalated rhodium(III) complexes $[Cp^{X}Rh(C^{\wedge}N)Z]^{0/+}$, in which Cp^{X} = Cp*, Cp^{ph}, or Cp^{biph}, C^N = benzo[*h*]quinoline, and Z = chloride or pyridine. Three X-ray crystal structures showing the expected "piano-stool" configurations have been determined. The chlorido complexes hydrolyzed faster in aqueous solution, and reacted preferentially with 9-ethyl guanine or glutathione compared to their pyridine analogues. The 1-biphenyl-2,3,4,5-tetramethylcyclopentadienyl complex $[Cp^{biph}Rh$(benzo-[*h*]quinoline)Cl] (**3a**) was the most efficient catalyst in coenzyme reduced nicotinamide adenine dinucleotide (NADH) oxidation to NAD^{+} and induced an elevated level of reactive oxygen species (ROS) in A549 human lung cancer cells. The pyridine complex $[Cp^{biph}Rh$(benzo[*h*]quinoline)-py$]^{+}$ (**3b**) was the most potent against A549 lung and A2780 ovarian cancer cell lines, being 5-fold more active than cisplatin towards A549 cells, and acted as a ROS scavenger. This work highlights a ligand-controlled strategy to modulate the reactivity and cytotoxicity of cyclometalated rhodium anticancer complexes.

Introduction

The approval of cisplatin as an anticancer drug in the late 1970s has not only led to new generations of platinum drugs in clinical use (carboplatin and oxaliplatin) or trials, but also to the search for a new era of transition metal-based anticancer agents.[1–4] Group 9 metals iridium and rhodium have attracted much attention although are less widely studied than platinum.[5–8] Ir^{III} and Rh^{III} complexes with low spin d^6 configurations are usually considered to be kinetically inert, however, recent studies have revealed that their reactivity toward biological targets can be adjusted by the rational selection of the surrounding ligands directly coordinated to the metal.[6,9] Kinetically stable iridium/rhodium pyridocarbazole complexes have been synthesized by Meggers and co-workers as potent enzyme inhibitors,[10–13] and Sheldrick and co-workers have reported various pentamethyl-cyclopentadienyl (Cp*) iridium/rhodium complexes with chelating polypyridine ligands as potent anticancer agents.[14] More recently, attention has turned to cyclometalated iridium and rhodium complexes in which five-membered chelate rings contain a strong M–C σ bond.[15,16] Nevertheless, research on cyclometalated rhodium complexes has largely focused on non-cyclopentadienyl cyclometalated rhodium complexes that target DNA, enzyme or protein–protein interfaces.[5,9,17–20] Reported cyclopentadienyl rhodium anticancer complexes to date, have mainly contained N^N,[21,22] N^S,[23] N^O,[24–26] or O^O[22,27,28] chelating ligands.

Our recent work has demonstrated that replacing the N^N coordinating ligand 2,2′-bipyridine or 1,10-phenanthroline with C^N chelating 2-phenylpyridne or benzo[*h*]quinoline in pentamethyl-cyclopentadienyl (Cp*) iridium complexes, not only enhances nucleobase binding and lipophilicity, but also switches on anticancer activity towards human A2780 ovarian cancer cells.[29,30] Moreover, the chelated iridium(III) biphenyl-tetramethyl-cyclopentadienyl complex $[Cp^{biph}Ir$(phenylpyridine)-(pyridine)$]^{+}$ can utilize NADH as a hydride source to transfer hydride electrons to oxygen, generating hydrogen peroxide and reactive oxygen species in cancer cells to trigger cell death.[31] Recently, we have described rhodium anticancer complexes $[Cp^{X}Rh(N^{\wedge}N')Cl]^{+}$ (Cp^{X} = Cp*, Cp^{ph}, or Cp^{biph}) which can be effective transfer hydrogenation catalysts inducing reductive stress when co-administrated with a non-toxic dose of sodium formate as the hydride donor in cancer cells.[32] Intriguingly, the Cp^{X} ring in these catalytic $[Cp^{X}Rh(N^{\wedge}N')Cl]^{+}$ ($N^{\wedge}N'$ is the bipyridine, dimethylbipyridine, or phenanthroline) complexes can be readily activated by deprotonation and undergo rapid deuteration in aqueous media, so providing a novel activation pathway for half-sandwich Rh^{III} complexes.[33] Based on these interesting discoveries, we have extended our studies to include cyclometalated cyclopentadienyl rhodium anticancer complexes with potential catalytic properties.

Herein, six cyclometalated rhodium complexes (Scheme 1) bearing different cyclopentadienyl Cp^{X} rings with C^N chelating ligand benzo[*h*]quinoline have been synthesized and fully characterized by ^{1}H NMR, ^{13}C NMR, high resolution ESI-MS and elemental analysis. Five novel complexes **2a**, **3a**, **1b**–**3b** are reported, and the X-ray crystal structures of complexes **2a**, **3a** and **1b·PF_6** have been determined. Complexes **1a**–**3a** contain chloride, while complexes **1b**–**3b** feature pyridine as the

[a] *Department of Chemistry, University of Warwick, CV4 7AL, Coventry, UK*
E-mail: p.j.sadler@warwick.ac.uk
https://warwick.ac.uk/fac/sci/chemistry/research/sadler/
Supporting information and ORCID(s) from the author(s) for this article are available on the WWW under https://doi.org/10.1002/ejic.201901055.

monodentate ligand. Their aqueous chemistry including hydrolysis, binding to nucleobase 9-ethylguanine (9-EtG) or abundant cellular thiol glutathione (GSH, γ-L-Glu-L-Cys-Gly), as well as catalytic activity in the oxidation of coenzyme NADH are evaluated and compared. Cytotoxicity has been screened against human A549 lung and A2780 ovarian cancer cell lines. Cellular Rh accumulation, ROS induction and apoptosis in A549 cancer cells induced by complexes **3a** and **3b** at equipotent concentrations have been investigated to elucidate their possible mechanism of action.

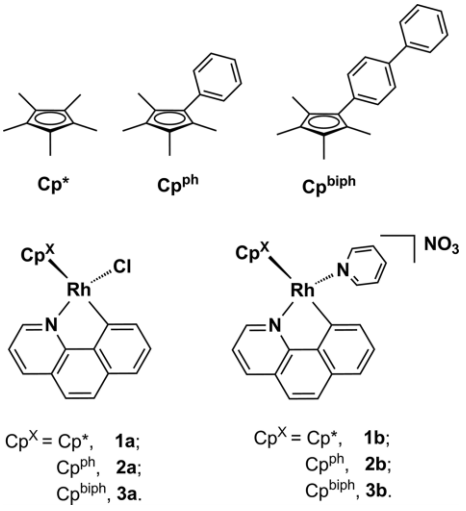

Scheme 1. Structures of the six cyclometalated rhodium(III) benzo[*h*]quinoline complexes studied in this work.

Results and Discussion

Synthesis and Characterization

The synthesis of the rhodium dimers $[Cp^XRh(\mu\text{-}Cl)Cl]_2$ (Cp^X = Cp^{ph}, Cp^{biph}) followed the reported procedure.[32,34] The rhodium chlorido complexes **1a**–**3a** were synthesized via C–H activation of benzo[h]quinoline by the rhodium dimer aided by sodium acetate in dichloromethane at ambient temperature as reported previously.[35] In contrast, pyridine complexes **1b**–**3b** were obtained in good yields through the reaction of the corresponding chlorido complexes with silver nitrate and then with excess pyridine (Scheme 2). All complexes were characterized by ^1H and ^{13}C NMR, elemental analysis and high resolution ESI-MS.

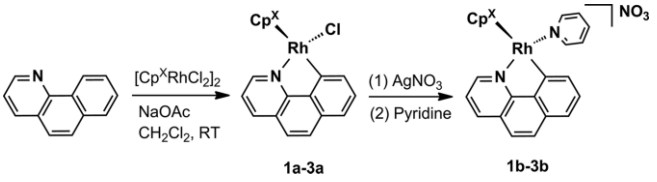

Scheme 2. Synthesis route for rhodium complexes containing chloride (**1a**–**3a**) and pyridine (**1b**–**3b**) ligands.

X-ray Crystal Structures

Crystal structures of $[Cp^{ph}Rh(benzo[h]quinoline)Cl]$ (**2a**), $[Cp^{biph}Rh(benzo[h]quinoline)Cl]$ (**3a**) and $[Cp^*Rh(benzo[h]quinoline)pyridine]PF_6$ (**1b·PF$_6$**) with PF_6^- as the counter anion were determined and are shown in Figure 1 with the atom numbering scheme. Crystallographic data are listed in Table S1, and selected bond lengths and angles in Table S2. All structures adopt the familiar "piano-stool" geometry. The distances between Rh and the centroid of the η^5-cyclopentadienyl ring are within 1.827–1.832 Å. The length of the Rh–C (quinoline) bond in **2a**, **3a**, **1b·PF$_6$** [2.050(3), 2.0458(15), 2.058(2), respectively] is significantly shorter than the Rh–N (quinoline) bond length [2.082(3), 2.1030(14), 2.1068(18), respectively].

Aqueous Solution Chemistry

The hydrolysis of these complexes was monitored by ^1H NMR (Figures 2, S1, S2) as well as UV/Vis spectroscopy at 310 K in methanol/water. Methanol was used to ensure sufficient solubility of the complexes in water. All the chlorido complexes showed faster hydrolysis than their pyridine analogues. Their hydrolysis rates and half-lives of hydrolysis (listed in Table 1) were determined by fitting the UV/Vis absorption changes vs. time to pseudo-first-order kinetics (Figure S6). With the exten-

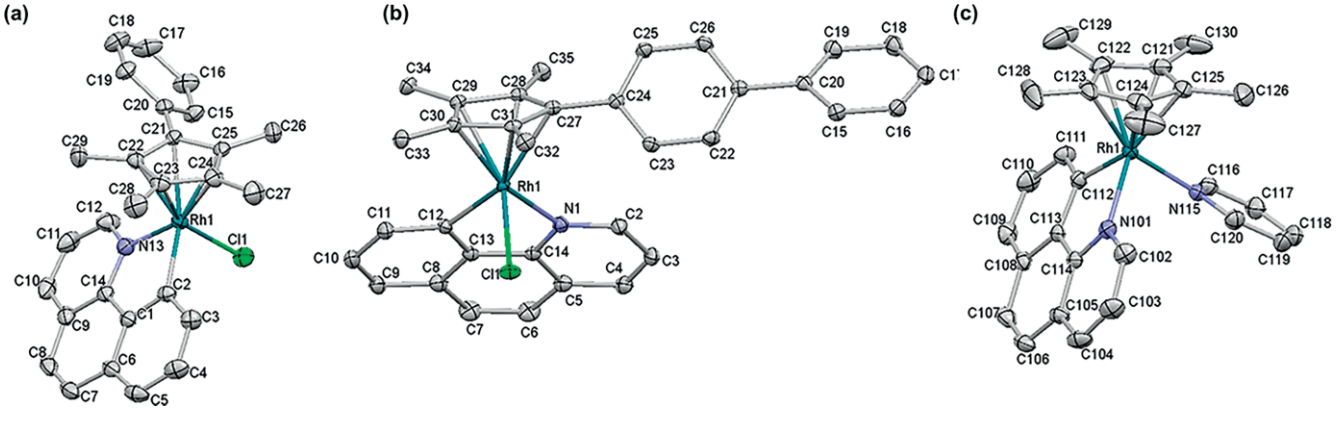

Figure 1. X-ray structures with atom numbering of (a) $[Cp^{ph}Rh(benzo[h]quinoline)Cl]$ (**2a**); (b) $[Cp^{biph}Rh(benzo[h]quinoline)Cl]$ (**3a**); (c) $[Cp^*Rh(benzo[h]quinoline)pyridine]PF_6$ (**1b·PF$_6$**), drawn with thermal ellipsoids at 50 % probability. Hydrogen atoms and counterions have been omitted for clarity.

sion of Cp* to Cp^{ph}, to Cp^{biph}, the hydrolysis half-lives of the chlorido complexes become shorter, while the hydrolysis half-lives of the pyridine complexes become longer. The hydrolysis extent over 24 h for chlorido complexes **1a**–**3a** was 43 %-60 % at equilibrium based on integration of ^{1}H NMR peaks. In addition, after 24 h, an additional set of ^{1}H NMR peaks was evident for complexes **1a**–**3a** which can be attributed to release of the benzo[*h*]quinoline ligand (ca. 25 %), as characterized by ^{1}H NMR, ^{1}H-^{1}H COSY and confirmed by ESI-MS with *m/z* 180.13 (calculated *m/z* 180.08) (Figures S7–S9). In contrast, after 24 h at 310 K, no apparent change was observed for millimolar solutions of the pyridine complexes **1b**–**3b** in [D$_4$]MeOD/D$_2$O (1:9–1:2 v/v) by ^{1}H NMR (Figures S3–S5), although the hydrolysis of micromolar solutions of complexes **1b**–**3b** could be observed by UV/Vis spectroscopy at 310 K (Figure S10).

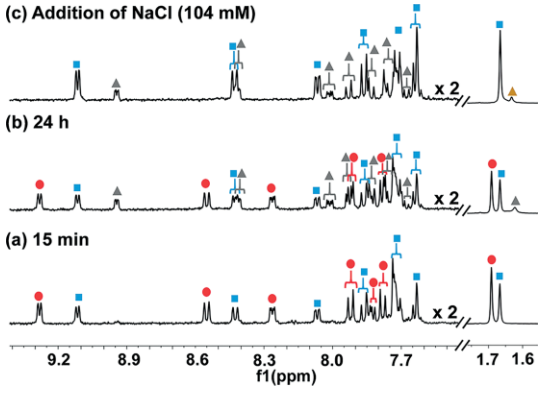

Figure 2. 400 MHz ^{1}H NMR spectra of [Cp*Rh(benzo[*h*]quinoline)Cl] (**1a**) (ca. 0.5 mM) in d$_4$-MeOH/D$_2$O (v/v 4:1) after (a) 15 min; (b) 24 h; and (c) 10 min after addition of NaCl (104 mM). After 15 min, 60 % of the parent complex **1a** (blue square) hydrolyzed to its aqua adduct [Cp*Rh(benzo[*h*]-quinoline)D$_2$O]$^+$ (red ball). After 24 h, one third of the aqua adduct [Cp*Rh(benzo[*h*]quinoline)D$_2$O]$^+$ had decomposed into the free chelated ligand and [Cp*Rh(D$_2$O)$_3$]$^{2+}$ (grey triangle). After addition of NaCl, all the aqua adducts were coverted into **1a**, with the released ligand remaining unbound and the [Cp*Rh(D$_2$O)$_3$]$^{2+}$ reacting with Cl$^-$ to form [Cp*RhCl$_2$]$_2$ (brown triangle).

Table 1. Hydrolysis data for complexes **1a**–**3a** and **1b**–**3b** at 310 K.

Complex	Cp^x	Extent[a]	k[b] (min^{-1})	$t_{1/2}$[b] (min)
1a	Cp*	43%	0.014 ± 0.002	49.7
2a	Cp^{ph}	50%	0.026 ± 0.002	26.8
3a	Cp^{biph}	60%	0.138 ± 0.016	5.0
1b	Cp*	0%	0.019 ± 0.001	36.0
2b	Cp^{ph}	0%	0.010 ± 0.001	70.0
3b	Cp^{biph}	0%	0.007 ± 0.001	95.9

[a] Determined by ^{1}H NMR in d$_4$-MeOH/D$_2$O. [b] At equilibrium, determined by UV/Vis spectroscopy in MeOH/H$_2$O.

When 104 mM NaCl (to mimic the chloride concentration in blood plasma), was added to the 24 h equilibrium hydrolysis solution of complexes **1a** (Figure 2c) and **2a** (Figure S1c), peaks for the aqua adducts disappeared and those for the parent chlorido complexes increased in intensity, confirming that hydrolysis of the chlorido complexes is reversible.

Interaction with 9-EtG

Reactions between chlorido/pyridine complexes and nucleobase 9-ethylguanine (9-EtG) were studied by ^{1}H NMR spectroscopy. Equimolar 9-EtG was added to an equilibrium solution of [Cp*Rh(benzo[*h*]quinoline)Cl] (**1a**) in [D$_4$]MeOD/D$_2$O (4:1, v/v, pH* 7.4) and the ^{1}H NMR spectra showed that ca. 90 % of **1a** had rapidly formed adducts with 9-EtG (within 20 min) based on the integral of the Cp* protons of **1a** (δ = 1.71 ppm), aqua adducts of **1a** (δ = 1.68 ppm) and 9-EtG adducts (δ = 1.66 ppm) (Figure 3). The new singlet peak for H8 of the bound 9-EtG appeared at 7.39 ppm, shifted by 0.37 ppm to high field relative to that of free 9-EtG. The ESI-MS spectra of the final NMR solution showed a major peak at *m/z* 595.3, assignable as the adduct of **1a** with 9-EtG [Cp*Rh(9-EtG)(benzo[*h*]quinoline)]$^+$ (calcd *m/z* 595.1). Meanwhile, in the presence of 4 mM NaCl, **1a** still showed a high affinity for 9-EtG with ca. 90 % **1a** binding to 9-EtG (Figure S11) at 310 K. Adducts of **2a** and **3a** with 9-EtG were also characterized by ^{1}H NMR (Figure S12) and ESI-MS (Table S3).

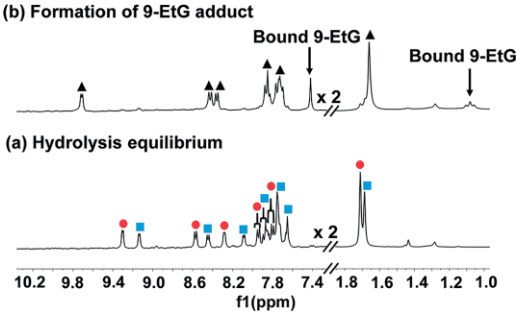

Figure 3. 300 MHz ^{1}H NMR spectra of (a) an equilibrium solution of ca. 1.0 mM complex [Cp*Rh(benzo[*h*]quinoline)Cl] (**1a**) in [D$_4$]MeOD/D$_2$O (4:1 v/v, pH* 7.4), containing both the chlorido complex **1a** (blue square) and its aqua adduct (red ball). (b) 20 min after addition of equimolar 9-EtG, ca. 90 % of **1a** had formed an adduct (black triangle) with 9-EtG.

By contrast, a ^{1}H NMR study of the pyridine complex [Cp*Rh(benzo[*h*]quinoline)py]NO$_3$ (**1b**) with equimolar 9-EtG in [D$_4$]MeOD/D$_2$O (1:4, v/v, pH* 7.4) showed that only 30 % of complex **1b** formed an adduct with 9-EtG after 24 h at 310 K (Figure 4) based on the integral of the Cp* methyl protons at 1.57 ppm (**1b**) and 1.56 ppm (9-EtG adduct with **1b**). This new adduct of complex **1b** with 9-EtG was also confirmed by the ESI-MS peak at *m/z* 595.3 (calcd *m/z* 595.1).

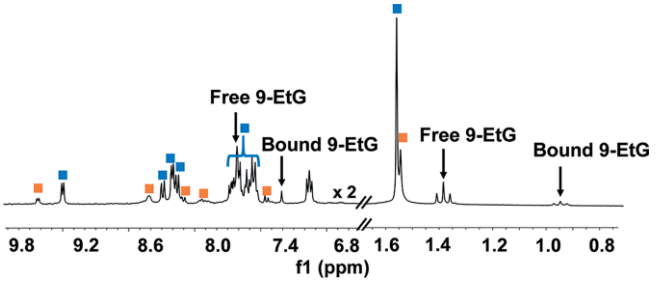

Figure 4. 300 MHz ^{1}H NMR spectrum of ca. 2.6 mM complex [Cp*Rh(benzo[*h*]quinoline)py]$^+$ (**1b**) (blue square) in [D$_4$]MeOD/D$_2$O (v/v 1:4, pH* 7.4) with equimolar 9-EtG after 24 h at 310 K. 30 % of complex **1b** formed an adduct (orange square) with 9-EtG.

NADH Oxidation

NADH is a crucial coenzyme in numerous biological catalytic processes. Previously, we have found that cyclopentadienyl iridium complexes bearing N^N coordinating ligands can accept hydride from NADH and induce the reduction of protons to H_2,[36] and quinones to semiquinones.[37] The 1-biphenyl-2,3,4,5-tetramethylcyclopentadienyl (Cp^{biph}) iridium complex with the C^N chelating 2-phenylpyridine can also transfer hydride from NADH to oxygen to produce the reactive oxygen species (ROS) hydrogen peroxide.[31] Therefore, the time dependence of reactions between rhodium complexes (0.8 μM) and NADH (75–144 μM) was studied over 24 h in 1.6 % MeOH/98.4 % phosphate buffer (5 mM, pH 7.4) by UV/Vis spectroscopy at 310 K (Figures S13, S14). The reactions proceeded via first-order kinetics (Figure S15).

The turnover number (TON) and turnover frequency (TOF) were determined based on the decrease in absorption of NADH at 339 nm due to conversion of NADH to NAD^+. In reactions with NADH at a higher concentration (144 μM), pyridine complexes **1b**–**3b** showed a much lower TOF than their respective chlorido analogues **1a**–**3a** (Table 2). This might due to the decrease in hydrolysis of pyridine complexes compared to chlorido analogues, as hydrolysis is believed to be the first step in interactions with NADH.[31] In the presence of 75 μM or 117 μM NADH, complex **3a** bearing a Cp^{biph} ring showed a ca. 2.6 × or ca. 2.3 ×, respectively, higher TOF than the other chlorido complexes **1a** and **2a**. In contrast, in the presence of 144 μM NADH, pyridine complex **1b**, which has the fastest hydrolysis rate among all these pyridine complexes, exhibited the highest TON and TOF. Furthermore, hydrogen peroxide was detected (appearance of blue color on Quantofix test sticks) in the reaction mixture of complex **3a** (ca. 1 mM) with 3.5 mol equiv. NADH in MeOH/H_2O (1:1 v/v) after 24 h at 310 K (Figure S16).

Table 2. TONs and TOFs for rhodium complexes (0.8 μM) in the catalytic oxidation of NADH to NAD^+ in 1.6 % MeOH/98.4 % phosphate buffer (5 mM, pH 7.4) over 24 h at 310 K.

Complex	NADH (μM)	TON	TOF (h^{-1})
1a	75	13	1.16 ± 0.06
	117	49	3.35 ± 0.11
2a	75	14	1.10 ± 0.08
	117	51	3.38 ± 0.15
3a	75	32	2.85 ± 0.12
	117	58	7.58 ± 0.20
1b	144	72	2.85 ± 0.06
2b	144	35	1.63 ± 0.02
3b	144	49	1.73 ± 0.04

Sodium Formate as Hydride Donor

Inspired by the ability of half-sandwich rhodium(III) complexes with N^N chelating ligands to act as transfer hydrogenation catalysts using sodium formate as a hydride source and convert pyruvate to lactate,[32] the ability of complex [Cp*Rh(benzo[*h*]quinoline)Cl] (**1a**) to reduce pyruvate to lactate was investigated. Upon addition of 10 mol equiv. sodium formate to a solution of **1a** in [D_4]MeOD/H_2O (99:1 v/v), the color turned from orange to red. In the hydride region, a ^1H NMR doublet appeared at −12.26 ppm [$J(^1H\text{-}^{103}Rh)$ = 32 Hz, Figure S17] which can be assigned to the hydride complex [Cp*Rh(H)(benzo[*h*]quinoline)] in accord with the reported *J* value[38] for the same Rh–H species. Meanwhile, a triplet at −19.34 ppm (*J* = 24 Hz) was also observed in Figure S17. The *J* value of this triplet is characteristic of hydride bridging two Rh^{III} centers,[39] suggesting a possible nucleophilic attack of the Rh–H bond on the labile coordination site occupied by MeOD or H_2O on another Rh molecule. Subsequently, when 5 mol equiv. pyruvate was added to this Rh-hydride solution, ca. 17 % of pyruvate (δ = 2.36 ppm, singlet) was reduced to lactate (δ = 1.32 ppm, doublet) based on ^1H NMR peak integrals over 24 h at 310 K (Figure S18).

Reactivity with GSH

The abundant cellular tripeptide glutathione (GSH) is a detoxification agent and ROS scavenger. Reactions between complex [Cp^{biph}Rh(benzo[*h*]quinoline)Cl] (**3a**)/pyridine analogue [Cp^{biph}Rh(benzo[*h*]quinoline)py]$^+$ (**3b**) and GSH were investigated. LC–MS analysis of **3b** with 2 mol equiv. GSH in MeOH/H_2O (1:9 v/v) revealed that most of the parent complex **3b** remained intact within the first 30 min, but after 18 h, **3b** was converted into dinuclear [$(Cp^{biph}Rh)_2(\mu\text{-}SG)_3$]$^+$ adducts (Figure S19). However, under the same conditions, the chlorido complex **3a** formed [Cp^{biph}Rh(SG) + H]$^+$ as detected by ESI-MS with *m/z* 683.6 (calcd 683.6) as soon as it was mixed with GSH. These differences in reactions with GSH may have a significant effect on the anticancer activity of these two complexes.

Cytotoxicity

The anticancer activity of rhodium complexes against human A549 lung and A2870 ovarian cancer cell lines was evaluated in vitro using the SRB assay after 24 h treatment and subsequent 72 h of cell recovery. The detailed half maximal inhibitory concentration (IC_{50}) values are listed in Table S4 and shown in Figure 5. Compared to cisplatin (CDDP) as the positive control, chlorido complexes **1a**–**3a** and pyridine complexes **1b**–**2b** all showed antiproliferative activity towards these two cell lines. In particular, the pyridine complex [Cp^{biph}Rh(benzo[*h*]quinoline)py]NO_3 (**3b**) exhibited the highest activity among all the screened rhodium complexes, ca. 5 × greater potency than cisplatin against A549 lung cancer cells.

In the study of cyclopentadienyl iridium complexes with the C^N chelating ligand 2-phenylpyridine, the extension of Cp^X (from Cp* to Cp^{ph} to Cp^{biph}) greatly enhanced the anticancer activity, perhaps due to the increased lipophilicity facilitating passage through the cell membrane, or to the extended phenyl or biphenyl ring which can intercalate between DNA bases.[40] Among the Cp^X analogues, Cp^{biph} capped complexes **3a** and

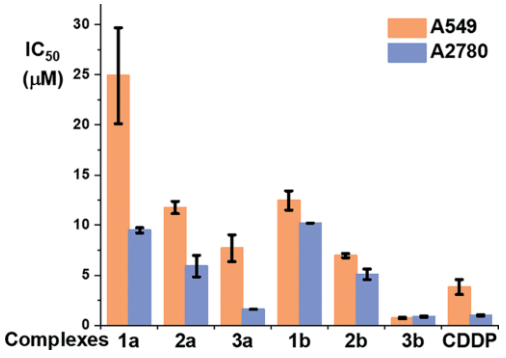

Figure 5. Anticancer activity of rhodium complexes towards human A549 lung and A2780 ovarian cancer cells in comparison with cisplatin (CDDP). The values of half maximal growth inhibitory concentration (IC_{50}) were determined by SRB assay and given as the mean ± standard deviations for three independent experiments. Stock solutions of tested complexes were prepared with 0.5 % v/v DMSO and the drug-treatment period was 24 h.

3b were the most hydrophobic and exhibited the highest potency as expected. Moreover, pyridine complex **3b** was ca. 2 × and ca. 10 × more potent than its chlorido analogue **3a** towards A2780 and A549 cancer cells, respectively (A2780: IC_{50} 0.88 μM for **3b** and 1.60 μM for **3a**; A549: IC_{50} 0.74 μM for **3b** and 7.69 μM for **3a**). Therefore, despite the replacement of the chloride with pyridine decreasing hydrolysis, inhibiting adduct formation with 9-EtG/GSH and lowering the catalytic TOF, the in vitro anticancer activity of pyridine complexes was higher than that of chlorido analogues, in line with the behavior of cyclometalated iridium pyridine complexes which showed slower hydrolysis/less interaction with biomolecules, but higher potency than their chlorido analogues.[31]

Cellular Rh Accumulation

Complexes [Cp^{biph}Rh(benzo[*h*]quinoline)Cl] (**3a**) and [Cp^{biph}Rh(benzo[*h*]quinoline)py]NO_3 (**3b**) bearing the Cp^{biph} ring, were the most potent candidates among the chlorido family **1a**–**3a** and pyridine family **1b**–**3b**. However, complex **3b** is positively charged and 10 × more potent than neutral complex **3a** towards A549 cancer cells (Figure 5). Thus, to elucidate their different anticancer activities, the cellular accumulation of rhodium in A549 human lung cancer cells after 24 h treatment with complexes **3a** and **3b** at equipotent concentrations of 0.5 × and 1 × IC_{50} at 310 K was quantified by Inductively Coupled Plasma - Mass Spectrometry (ICP-MS) as shown in Figure 6 (values in Table S5). From Figure 6, the accumulation of Rh in the cells treated with complex **3a** or **3b** increased in a concentration-dependent manner. After 24 h the cellular Rh accumulation of chlorido complex **3a** was ca. 49-fold (at 0.5 × IC_{50}) and ca. 59-fold (at 1 × IC_{50}) higher than that of complex **3b**. This significant difference correlates with the higher hydrophobicity of neutral complex **3a** compared to the positive complex **3b**, in contrast to the reported cyclometalated iridium complex [Cp^{biph}Ir(2-phenylpyridine)py]$^+$ which was found to have 20-fold higher Ir accumulation than the neutral iridium complex [Cp^{biph}Ir(2-phenylpyridine)Cl] in A2780 cancer cells.[31]

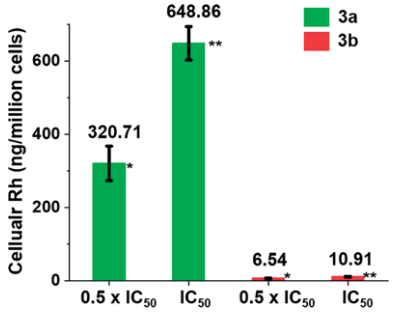

Figure 6. Accumulation of Rh (ng/million cells) in A549 human lung cancer cells after 24 h treatment with chlorido complex **3a** or pyridine complex **3b** at concentrations of 0.5 × IC_{50} and 1 × IC_{50}. The values represent mean ± standard deviations for three independent samples. The asterisk denotes the *p*-values obtained by comparing each dataset with the negative control (untreated cells) using a t-test, $^*p < 0.05$, $^{**}p < 0.01$.

ROS Induction in A549 Cancer Cells

The chlorido complexes **1a**–**3a** exhibited higher catalytic efficiency than pyridine analogues in the oxidation of NADH to NAD^+ with production of hydrogen peroxide. We investigated whether these catalytic chlorido complexes can induce a high level of reactive oxygen species (ROS) in A549 human lung cancer cells after 24 h treatment with complexes [Cp^{biph}Rh(benzo[*h*]quinoline)Cl] (**3a**) and [Cp^{biph}Rh(benzo[*h*]quinoline)-

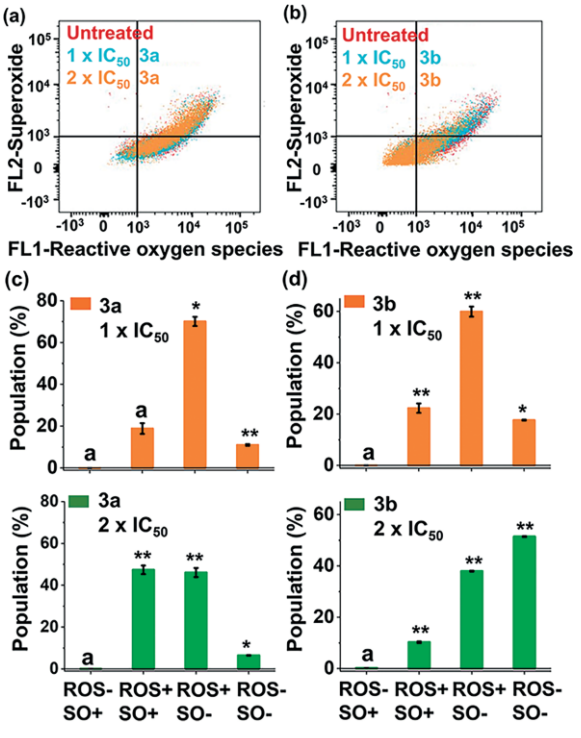

Figure 7. Flow cytometry plots of total ROS and superoxide production after 24 h treatment with 1 × and 2 × IC_{50} concentrations of complexes (a) **3a** and (b) **3b**. Cell populations of total ROS and superoxide production after 24 h treatment with 1 × and 2 × IC_{50} concentrations of complexes (c) **3a** and (d) **3b**. The values represent mean ± standard deviations for three independent samples. The asterisk denotes the *p*-values obtained by comparing each dataset with the negative control (untreated cells) using a t-test, $^*p < 0.05$, $^{**}p < 0.01$, $^a p > 0.05$.

py]NO_3 (**3b**) at concentrations of IC_{50} or 2 × IC_{50} by flow cytometry analysis using a total ROS/Superoxide detection kit (Figure 7, details in Table S6). This assay not only allowed determination of the level of total ROS consisting of H_2O_2, peroxy and hydroxyl radicals, peroxynitrite, and NO species, but also the level of superoxide (SO). After 24 h drug treatment, a concentration-dependent ROS level modulation indicated by the fluorescence signals of FL1 (indicating the total ROS level) and FL2 (indicating the SO level) channels was observed: in cells treated with complex **3a**, the ROS+/SO+ cell population increased significantly from 18 ± 2 % at IC_{50} concentration to 47 ± 2 % at 2 × IC_{50} concentration of complex. In contrast, for cells treated with complex **3b**, the cell population producing ROS decreased significantly from 60 ± 2 % (ROS+/SO-)/22 ± 2 % (ROS+/SO+) by IC_{50} concentration treatment to 38 ± 0.1 (ROS+/SO-)/10 ± 0.3 (ROS+/SO+) by 2 × IC_{50} concentration treatment, combined with an increase in the quadrant of ROS-/SO- from 17 ± 0.2 % to 51 ± 0.2 (Figure 7, Table S6). This observation suggested opposing mechanisms of action for the two complexes: complex **3a** inducing ROS formation, complex **3b** acting as a ROS scavenger.

Apoptosis Assay

Apoptosis is well recognized as a distinct cell death mechanism in tumors responding to anticancer therapies.[41] To investigate whether apoptosis is involved in the anticancer activity, A549 cells were treated with [Cp^{biph}Rh(benzo[*h*]quinoline)Cl] (**3a**) and [Cp^{biph}Rh(benzo[*h*]quinoline)py]NO_3 (**3b**) at their equipotent concentrations of IC_{50} and 2 × IC_{50} for 24 h, then stained with FITC labelled-annexin V/propidium iodide (PI) and analyzed by flow cytometry. This assay determined cell populations as early apoptosis (annexin V+/PI–, stained by annexin V only), late apoptosis (annexin V+/PI+, stained by annexin V and PI), necrosis (annexin V–/PI+, stained by PI only), and viable (annexin V–/PI–, unstained by annexin V and PI). No obvious induction of apoptosis by complex **3a** or **3b** was observed at equipotent concentrations (Figure S20). However, there was a significant increase in necrotic cell population induced by the treatment with complex **3b** at 2 × IC_{50} concentration (Table S7).

Conclusions

In summary, we have described the synthesis and characterization of novel cyclopentadienyl C^N chelated Rh^{III} anticancer complexes. The reactivity and cytotoxicity of these complexes can be reasonably modulated by selection of the monodentate ligand as chloride or pyridine. The hydrolysis rate of chlorido complexes increases in the order Cp^* Cp^{ph} < Cp^{biph}, showing that incorporation of the extended Cp^X ring confers more labile kinetics on the monodentate chloride ligand. On the contrary, when the chloride is replaced with pyridine, the rate of hydrolysis is slowed down by orders of magnitude and decreases in the order Cp^* > Cp^{ph} > Cp^{biph}. This difference in hydrolysis kinetics for the chlorido and pyridine complexes leads to the differences in reactivity, and subsequent differences in cytotoxicity.

The pyridine complex **3b** reacts more slowly with glutathione than the chlorido analogue, resulting in less deactivation and an order of magnitude greater potency towards lung cancer cells. Meanwhile, complex **3b** accumulates to a much lesser extent than the chlorido analogue in cancer cells at equipotent IC_{50} concentrations, indicating that complex **3b** requires a lower dose than **3a** to achieve the same therapeutic potency. Significantly, the rhodium complexes studied here exhibit a different mechanism of action from cisplatin, which acts through interaction with DNA. The chlorido complex **3a** shows the greatest catalytic efficiency in NADH oxidation and induces a remarkable increase in the level of ROS in lung cancer cells. Whereas the pyridine complex **3b** can act as a ROS scavenger, which is distinct from the related pyridine iridium complex [Cp^{biph}Ir(2-phenylpyridine)py]$^+$ which induces a higher level of ROS in ovarian cancer cells.[31] Although the reason for the ROS scavenging activity is not clear, pyridine complex **3b** is the first example of an organometallic rhodium complex with such a behavior. Cyclometalated rhodium complexes such as these may provide a new generation of transition metal-based chemotherapeutic agents and are worthy of further investigation.

Experimental Section

Materials

Rhodium(III) trichloride hydrate was purchased from Precious Metals Online (PMO Pty Ltd.) and used as received. [Cp*Rh(μ-Cl)Cl]$_2$, benzo[*h*]quinoline, silver nitrate, sodium formate, sodium pyruvate, β-nicotinamide adenine dinucleotide reduced disodium salt (NADH), and Celite were purchased from Sigma-Aldrich. [D_4]MeOD, D_2O, and [D_1]$CDCl_3$ for NMR spectroscopy and Quantofix® peroxides test sticks (1–100 mg/L range) were purchased from Sigma-Aldrich. Reduced glutathione was obtained from Alfa Aesar. Disodium hydrogen phosphate dihydrate, disodium hydrogen phosphate dodecahydrate, anhydrous sodium acetate, HPLC grade solvents (water and acetonitrile) with added trifluoroacetic acid were analytical grade, anhydrous DCM/pyridine and laboratory grade solvents used in syntheses were purchased from Fisher Scientific. A549 human lung and A2780 human ovarian cancer cell lines were purchased from the European Collection of Animal Cell Culture (ECACC, Salisbury, U.K.). Roswell Park Memorial Institute (RPMI-1640) medium, and phosphate-buffered saline (PBS) were purchased from PAA Laboratories GmbH. The total ROS/superoxide detection kit was purchased from Enzo Life Sciences. The apoptosis detection regents were purchased from Abcam.

Synthesis

The dimeric rhodium precursors [Cp^{ph}Rh(μ-Cl)Cl]$_2$, [Cp^{biph}Rh(μ-Cl)Cl]$_2$ and complex [Cp^*Rh(benzo[*h*]quinoline)Cl] (**1a**) were synthesized according to the literature.[32,34,35]

Synthesis of [Cp^XRh(benzo[*h*]quinoline)Cl] (2a and 3a)

General procedure: [Cp^XRh(μ-Cl)Cl]$_2$ (0.12 mmol) with benzo[*h*]quinoline (0.36 mmol) and anhydrous sodium acetate (0.98 mmol) in 20 mL anhydrous DCM was stirred under nitrogen 48 h. Then the solution was filtered through celite and purified using a 10 g silica cartridge on a Biotage Isolera instrument (methanol/dichloromethane, 5:95 v/v). Then column-purified powder was recrystallized from dichloromethane/diethyl ether at 277 K to give a red crystalline solid.

[Cp^{ph}Rh(benzo[*h*]quinoline)Cl] (2a): 43 mg, yield 70 %; ^{1}H NMR (500 MHz, $CDCl_3$, 298 K): δ = 8.69 (d, J = 5.1 Hz, 1H), 8.14 (d, J = 8.0 Hz, 1H), 7.97 (d, J = 6.7 Hz, 1H), 7.79 (d, J = 8.7 Hz, 1H), 7.62–7.53 (m, 5H), 7.43–7.3 (m, 4H), 1.85 (s, 3H), 1.78 (s, 3H), 1.75 (s, 3H), 1.45 (s, 3H); ^{13}C NMR (125 MHz, $CDCl_3$, 298 K): δ = 175.18 ($J_{C\text{-}Rh}$ = 33.8 Hz), 155.32, 149.49, 140.54, 135.64, 133.83, 133.54, 131.99, 130.89, 129.71, 128.79, 127.77, 127.21, 123.13, 121.53, 121.32, 107.6, 100.31, 95.87, 94.64, 88.79, 10.84, 10.48, 9.54, 9.22. HR-MS (ESI): *m/z* calcd. for [Cp^{ph}Rh(benzo[*h*]quinoline)]$^+$: 478.1037, found 478.1032; elemental analysis calcd. (%) for $C_{28}H_{25}ClRhN$: C, 65.45; H, 4.90; N, 2.73; found C, 64.55; H, 4.86; N, 2.69.

[Cp^{biph}Rh(benzo[*h*]quinoline)Cl] (3a): 41 mg, yield 58 %; ^{1}H NMR (500 MHz, $CDCl_3$, 298 K): δ = 8.73 (d, J = 5.1 Hz, 1H), 8.14 (d, J = 7.9 Hz, 1H), 8.00 (d, J = 6.9 Hz, 1H), 7.80 (d, J = 8.7 Hz, 1H), 7.68–7.55 (m, 9H), 7.48 (t, J = 7.6 Hz, 2H), 7.40–7.34 (m, 2H), 1.89 (s, 3H),1.80 (s, 3H), 1.77 (s, 3H), 1.50 (s, 3H); ^{13}C NMR (125 MHz, $CDCl_3$, 298 K): δ = 175.14 ($J_{C\text{-}Rh}$ = 33.8 Hz), 155.30, 149.51, 140.59, 140.54, 140.31, 135.66, 133.83, 133.53, 131.26, 131.02, 130.20, 129.71, 129.04, 127.65, 127.36, 127.21, 127.11, 123.14, 121.59, 121.34, 107.56, 100.39, 95.44, 94.73, 88.91, 10.91, 10.53, 9.54, 9.23. HR-MS (ESI): *m/z* calcd. for [Cp^{biph}Rh(benzo[*h*]quinoline)]$^+$ 554.1350, found 554.1353; elemental analysis calcd. (%) for $C_{34}H_{29}ClRhN$: C, 69.22; H, 4.95; N, 2.37; found C, 69.31; H, 4.96; N, 2.17.

Synthesis of [Cp^{X}Rh(benzo[*h*]quinoline)py]NO$_3$ (1b–3b)

General procedure: [Cp^{X}Rh(benzo[*h*]quinoline)Cl] (0.05 mmol) was stirred with silver nitrate (0.05 mmol) in 10 mL methanol for 1.5 h. Then the solution was centrifuged and pyridine (0.5 mmol) was added to the upper clear layer. The color changed from orange to bright yellow, and the solution was stirred 24 h. Then the solution was concentrated, and product recrystallized from diethyl ether giving a yellow solid which was dried under vacuum.

[Cp*Rh(benzo[*h*]quinoline)py]NO$_3$ (1b): 18 mg, yield 65 %; ^{1}H NMR (500 MHz, [D$_4$]MeOD, 298 K): δ = 9.44 (d, J = 5.0 Hz, 1H), 8.54 (d, J = 7.4 Hz, 1H), 8.50 (d, J = 5.6 Hz, 2H), 8.35 (d, J = 7.2 Hz, 1H), 7.91–7.81 (m, 3H), 7.75–7.71 (m, 3H), 7.26 (t, J_1 = 6.8 Hz, J_2 = 7.3 Hz, 2H), 1.65 (s, 15H); ^{13}C NMR (125 MHz, [D$_4$]MeOD, 298 K): δ = 175.14 ($J_{C\text{-}Rh}$ = 35.0 Hz), 155.99, 154.20, 151.45, 141.71, 140.14, 138.82, 135.17, 134.29, 131.98, 130.77,128.77, 127.51, 124.94, 124.35, 123.77, 98.62, 9.04. HR-MS (ESI): *m/z* calcd. for [Cp*Rh(benzo[*h*]quinoline)-pyridine]$^+$ 495.1302, found 495.1297; elemental analysis calcd. (%) for $C_{28}H_{28}RhN_3O_3$: C, 60.33; H, 5.06; N, 7.54; found C, 59.65; H, 4.98; N, 7.50.

[Cp^{ph}Rh(benzo[*h*]quinoline)py]NO$_3$ (2b): 23 mg, yield 74 %; ^{1}H NMR (500 MHz, [D$_4$]MeOD, 298 K): δ = 9.22 (d, J = 5.0 Hz, 1H), 8.53–8.50 (m, 3H), 8.27 (d, J = 6.8 Hz, 1H), 7.91 (d, J = 8.7 Hz, 1H), 7.82–7.74 (m, 5H), 7.30 (t, J_1 = 6.7 Hz, J_2 = 7.4 Hz, 2H), 7.26 (d, J = 7.5 Hz, 1H), 7.16 (t, J_1 = 7.8 Hz, J_2 = 7.6 Hz, 2H), 6.90 (d, J = 7.3 Hz, 2H), 1.90 (s, 3H), 1.76 (s, 3H), 1.71 (s, 3H), 1.68 (s, 3H); ^{13}C NMR (125 MHz, [D$_4$]MeOD, 298 K): δ = 175.69 ($J_{C\text{-}Rh}$ = 33.8 Hz), 155.82, 154.29, 151.54, 141.54, 140.40, 138.98, 135.38, 134.38, 132.14,131.63, 131.02,130.85, 129.63, 129.43, 129.02, 127.72, 125.10, 124.27, 124.06, 105.56, 102.90, 102.08, 98.47, 93.07, 10.52, 10.35, 9.00. HR-MS (ESI): *m/z* calcd. for [Cp^{ph}Rh(benzo[*h*]quinoline)pyridine]$^+$ 557.1459, found 557.1458; elemental analysis calcd. (%) for $C_{33}H_{30}RhN_3O_3$: C, 63.98; H, 4.88; N, 6.78; found C, 63.91; H, 4.84; N, 6.76.

[Cp^{biph}Rh(benzo[*h*]quinoline)py]NO$_3$ (3b): 22 mg, yield 63 %; ^{1}H NMR (500 MHz, [D$_4$]MeOD, 298 K): δ = 9.24 (d, J = 5.1 Hz, 1H), 8.54 (d, J = 5.6 Hz, 2H), 8.51 (d, J = 8.0 Hz, 1H), 8.30 (d, J = 7.0 Hz, 1H), 7.91 (d, J = 6.7 Hz, 1H), 7.83–7.74 (m, 5H), 7.53 (d, J = 7.4 Hz, 2H), 7.43 (d, J = 8.2 Hz, 2H), 7.39 (t, J_1 = 7.4 Hz, J_2 = 7.7 Hz, 2H), 7.33–7.28 (m, 3H), 6.99 (d, J = 8.2 Hz, 2H),1.93 (s, 3H), 1.77 (s, 3H), 1.73 (s, 3H), 1.71 (s, 3H); ^{13}C NMR (125 MHz, [D$_4$]MeOD, 298 K): δ = 175.67 ($J_{C\text{-}Rh}$ = 33.8 Hz), 155.81,154.29, 151.59, 142.40, 141.54, 141.21,140.40, 139.00, 135.38, 134.40, 132.16, 131.55, 130.84, 130.57, 129.97, 129.02, 128.79, 149.49, 140.54, 135.64, 133.83, 133.54, 131.99, 130.89, 129.71, 128.79, 128.05, 127.82, 127.73, 126.12, 125.13, 124.35, 124.07, 105.50, 102.72, 101.93, 98.28, 93.41, 10.57, 10.43, 9.02, 9.01. HR-MS (ESI): *m/z* calcd. for [Cp^{biph}Rh(benzo-[*h*]quinoline)pyridine]$^+$ 633.1772, found 633.1768; elemental analysis calcd. (%) for $C_{39}H_{34}RhN_3O_3$: C, 67.34; H, 4.93; N, 6.04; found C, 67.25; H, 4.86; N, 5.95.

Methods and Instrumentation

X-ray Crystallography: Suitable crystals were selected and mounted on a glass fibre with Fomblin oil and placed on an Xcalibur Gemini diffractometer with a Ruby CCD area detector. The crystals were kept at 150(2) K, except crystal of complex **3a** at 100(2) K, during data collection. Using Olex2,[42] all the structures were solved with the ShelXT[43] structure solution program using direct methods and refined with the ShelXL[44] refinement package using least-squares minimization.

CCDC 1952984 (for **2a**), 1952985 (for **3a**), and 1952986 (for **1b·PF$_6$**) contain the supplementary crystallographic data for this paper. These data can be obtained free of charge from The Cambridge Crystallographic Data Centre.

NMR Spectroscopy: ^{1}H and ^{13}C NMR spectroscopy and ^{1}H-^{1}H gs (gradient selected) COSY(correlation spectroscopy), ^{1}H-^{13}C HMQC (heteronuclear multiple quantum coherence) and HMBC (heteronuclear multiple bond coherence) were acquired at 298 K (unless stated otherwise) on Bruker Advance 300 MHz, Bruker Advance III HD 500 MHz or 600 MHz NMR spectrometers. ^{1}H NMR chemical shifts were internally referenced to $CHCl_3$ (7.26 ppm) for [D]chloroform and $(CHD_2)OD$ (3.31 ppm) for [D$_4$]methanol. ^{13}C NMR chemical shifts were internally referenced to $CDCl_3$ (77.16 ppm) for [D]chloroform, and CD_3OD (49.00 ppm) for [D$_4$]methanol. The data were processed using Mestronova and Topspin (version 2.1 Bruker UK Ltd.).

Electrospray Mass Spectrometry: Electrospray ionization mass spectra (ESI-MS) were obtained by injecting the samples in methanol into a Bruker Esquire 2000 spectrometer. The mass spectra were recorded with a scan range of *m/z* either 50–500 or 400–1000 for positive ion mode. HR-MS analysis was carried with a Bruker MaXis plus Q-TOF mass spectrometer equipped with electrospray ionization source. The mass spectrometer was operated in electrospray positive ion mode with a scan range 50–2,400 *m/z*.

Elemental Analysis: CHN elemental analyses were carried out on a CE-440 elemental analyzer by Warwick Analytical (UK) Ltd.

pH Measurements: pH or pH* (pH meter reading without correction for effect of deuterium on the sensor) values of samples in H_2O or D_2O were measured at ca. 298 K, using a HATCH minilab pocket pH meter with ISFET (silicon chip) sensor, calibrated with buffer solutions of pH 4, 7, and 10.

UV/Vis Spectroscopy: A Cary 300 UV/Vis recording spectrophotometer was used with 1 cm path-length quartz cuvettes (3.0 mL) and a PTP1 Peltier temperature controller. Experiments were carried out at 310 K from 800 to 200 nm in 0.5 nm intervals unless stated otherwise. Spectra were recorded using UV Winlab software and analyzed using Origin 2018.

Reactions with NADH: The time dependence of reactions of rhodium complexes (0.8 μM) with NADH (75–144 μM) were studied over 24 h in 1.6 % MeOH-98.4 % phosphate buffer (5 mM, pH 7.4) by UV/Vis spectroscopy at 310 K. The concentration of NADH was obtained

using the extinction coefficient ε(339 nm) = 6220 M^{-1} cm^{-1}.[31] TON was calculated from the difference in NADH concentration divided by the concentration of metal complex catalyst over 24 h. TOF was calculated from the linear fitting of TON vs. time (h) by Origin 2018.

Inductively Coupled Plasma-Optical Emission Spectroscopy (ICP-OES): ICP-OES analysis was carried out on a PerkinElmer Optima 5300 DV series Optical Emission Spectrophotometer. The Rhodium Specpure® plasma standard (Alfa Aesar, 1000 µg/mL in 20 % v/v HCl) was diluted with ca. 3.6 % HNO_3 Milli-Q water to provide freshly prepared calibrants at concentrations of 700, 600, 500, 400, 300, 200, 100, 50, and 0 ppb, which were adjusted to match the sample matrix by standard addition of sodium chloride (TraceSELECT®). Total dissolved solids did not exceed 0.2 % w/v. Data were acquired and processed using WinLab32 V3.4.1 for Windows.

ICP-MS: The whole cell pellet was digested in 72 % nitric acid at 353 K overnight. Samples after digestion were diluted to give a final concentration of ca. 3.6 % nitric acid and analyzed using an ICP-MS Agilent Technologies 7500 series in no-gas/helium mode. ICP-MS TOP and Offline Data Analysis (ChemStation version B.03.05) by Agilent Technologies were used to process the data. Biological triplicates were produced for each sample and statistical significance was calculated (Welch's unpaired t-test).

High-Performance Liquid Chromatography (HPLC)/LC-MS: Reverse phase HPLC (RP-HPLC) was performed on a HP 1100 Series HPLC System (Agilent) using a ZORBAX Eclipse Plus C-18 column (250 × 4.6 mm, 5 µm). Eluents: A-water (0.1 % v/v TFA), B-acetonitrile (0.1 % v/v TFA). Solvent gradient method: 0–30 min, 10 %-80 % B; 30–40 min, 80 % B; 40–41 min, 80 %-10 % B; 40–55 min, 10 % B. A flow rate of 1 mL min^{-1} was used with detection wavelength at 254 nm. LC-MS was carried out on a Bruker Amazon X connected online to an Agilent 1260 HPLC with detection wavelength 254 nm. The mobile phases and the solvent gradient method were the same as HPLC.

Cell Culture: A549 human lung cell line and A2780 human ovarian cell line were grown in RPMI-1640 with L-glutamine supplemented with 10 % v/v fetal bovine serum, and 1 % v/v penicillin/streptomycin. All cells were grown as adherent monolayers at 310 K with a 5 % CO_2 humidified atmosphere, and were passaged at ca. 80 % confluency.

Cell Viability Assay: Briefly, 5000 cells were seeded per well in 96-well plates. The cells were pre-incubated in drug-free media at 310 K for 48 h before adding different concentrations of test compounds. Stock solutions of the complexes were prepared in DMSO (< 0.5 %)/cell culture medium and the concentration of each metal complex in the stock solution was determined by ICP-OES. The drug exposure period was 24 h. After this, supernatants were removed by suction and each well was washed with 100 µL PBS. The cells were allowed a further 72 h recovery in compound-free fresh medium at 310 K. SRB assay was used to determine cell viability.[45] Absorbance measurements of the solubilized dye (on a BioRad iMark microplate reader using a 470 nm filter) allowed the determination of viable treated cells compared to untreated controls. IC_{50} values were determined as duplicates of triplicates in two independent sets of experiments and their standard deviations were calculated.

Cellular Rh Accumulation: The accumulation of Rh in A549 human lung carcinoma cells was determined by ICP-MS. 1×10^6 cells were seeded into a 100 mm Petri dish and incubated in drug-free media for 24 h at 310 K. For a further 24 h, the cells were incubated in media containing 0.5 × and 1 × IC_{50} concentrated complex **3a** or **3b**. Following this, cells were washed, detached using trypsin-EDTA, resuspended in fresh media, counted and centrifuged. The cell pellets were digested as ICP-MS protocol for Rh analysis.

ROS Determination: 5×10^4 A549 human lung carcinoma cells were seeded per well in a 6-well plate and incubated for 24 h at 310 K. 1 × or 2 × IC_{50} concentrated complex **3a** or **3b** was added to the cells and incubated for a further 24 h. After which, total ROS and SO concentrations were analyzed by flow cytometry using the total ROS/superoxide detection kit by Enzo Life Sciences. Briefly, the cells were enzymatically detached using trypsin-EDTA, washed in PBS, resuspended in staining solution, prepared according to manufacturer's instructions (25 nM concentration of both dyes, total ROS and SO) and incubated at room temperature for 30 min. Samples were then analyzed on the Beckton Dickinson LSRII using Beckton Dickinson FACSDIVA software. Data were processed using flowjo V10 for Windows. At all times, samples were kept under dark conditions to avoid light-induced ROS production. Welch's t-tests were carried out to establish statistical significance of the variations.

Apoptosis Assay: 5×10^4 A549 human lung carcinoma cells were seeded per well in a 6-well plate and incubated for 24 h at 310 K. 1 × or 2 × IC_{50} concentrated complex **3a** or **3b** was added to the cells and incubated for a further 24 h. After which, the cells were enzymatically detached using trypsin-EDTA, washed in PBS, resuspended in staining solution (FITC Annexin V diluted 1 in 100 and 1 µg/mL PI) and incubated at room temperature for 30 min. Samples were then analyzed on the Beckton Dickinson LSRII using Beckton Dickinson FACSDIVA software. Data were processed using flowjo V10 for Windows. Welch's t-tests were carried out to establish statistical significance of the variations.

Acknowledgments

This research was supported by the EPSRC (grant no. EP/P030572/1), Chancellor's International PhD Scholarships from the University of Warwick (for W.-Y. Z. and H. S.), an EPSRC and Mike Enfys Bagguley PhD studentship for H. E. B, a Royal Society-SERB Newton International Fellowship (NF151429 for S. B.), and the Wellcome Trust (209173/Z/17/Z for C. I.).

Keywords: Antitumor agents · Cyclopentadienyl ligands · Cytotoxicity · Rhodium · Reactive oxygen species

[1] P. Zhang, P. J. Sadler, *J. Organomet. Chem.* **2017**, *839*, 5–14.
[2] N. Shah, D. S. Dizon, *Future Oncol.* **2009**, *5*, 33–42.
[3] S. Dasari, P. B. Tchounwou, *Eur. J. Pharmacol.* **2014**, *740*, 364–378.
[4] M. Hanif, C. G. Hartinger, *Future Med. Chem.* **2018**, *10*, 615–617.
[5] C.-H. Leung, H.-J. Zhong, D. S.-H. Chan, D.-L. Ma, *Coord. Chem. Rev.* **2013**, *257*, 1764–1776.
[6] Y. Geldmacher, M. Oleszak, W. S. Sheldrick, *Inorg. Chim. Acta* **2012**, *393*, 84–102.
[7] G. Gasser, I. Ott, N. Metzler-Nolte, *J. Med. Chem.* **2011**, *54*, 3–25.
[8] Z. Liu, P. J. Sadler, *Acc. Chem. Res.* **2014**, *47*, 1174–1185.
[9] D.-Y. Zhang, Y. Zheng, H. Zhang, J.-H. Sun, C.-P. Tan, L. He, W. Zhang, L.-N. Ji, Z.-W. Mao, *Adv. Sci.* **2018**, *5*, 1800581.
[10] A. Wilbuer, D. H. Vlecken, D. J. Schmitz, K. Kräling, K. Harms, C. P. Bagowski, E. Meggers, *Angew. Chem. Int. Ed.* **2010**, *49*, 3839–3842; *Angew. Chem.* **2010**, *122*, 3928.
[11] L. Feng, Y. Geisselbrecht, S. Blanck, A. Wilbuer, G. E. Atilla-Gokcumen, P. Filippakopoulos, K. Kräling, M. A. Celik, K. Harms, J. Maksimoska, R. Marmorstein, G. Frenking, S. Knapp, L.-O. Essen, E. Meggers, *J. Am. Chem. Soc.* **2011**, *133*, 5976–5986.
[12] A. Kastl, A. Wilbuer, A. L. Merkel, L. Feng, P. Di Fazio, M. Ocker, E. Meggers, *Chem. Commun.* **2012**, *48*, 1863–1865.

[13] S. Dieckmann, R. Riedel, K. Harms, E. Meggers, *Eur. J. Inorg. Chem.* **2012**, *2012*, 813–821.
[14] M. A. Scharwitz, I. Ott, Y. Geldmacher, R. Gust, W. S. Sheldrick, *J. Organomet. Chem.* **2008**, *693*, 2299–2309.
[15] N. Cutillas, G. S. Yellol, C. de Haro, C. Vicente, V. Rodríguez, J. Ruiz, *Coord. Chem. Rev.* **2013**, *257*, 2784–2797.
[16] I. Omae, *Coord. Chem. Rev.* **2014**, *280*, 84–95.
[17] D.-L. Ma, M. Wang, Z. Mao, C. Yang, C.-T. Ng, C.-H. Leung, *Dalton Trans.* **2016**, *45*, 2762–2771.
[18] H. Liang, T. Hao, C. Yin, X. Yang, H. Fu, X. Zheng, R. Li, D. Xiao, H. Chen, *Eur. J. Inorg. Chem.* **2017**, *2017*, 4149–4157.
[19] G.-J. Yang, W. Wang, S. W. F. Mok, C. Wu, B. Y. K. Law, X.-M. Miao, K.-J. Wu, H.-J. Zhong, C.-Y. Wong, V. K. W. Wong, D.-L. Ma, C.-H. Leung, *Angew. Chem. Int. Ed.* **2018**, *57*, 13091–13095; *Angew. Chem.* **2018**, *130*, 13275.
[20] D.-L. Ma, L.-J. Liu, K.-H. Leung, Y.-T. Chen, H.-J. Zhong, D. S.-H. Chan, H.-M. D. Wang, C.-H. Leung, *Angew. Chem. Int. Ed.* **2014**, *53*, 9178–9182; *Angew. Chem.* **2014**, *126*, 9332.
[21] A. Gilewska, B. Barszcz, J. Masternak, K. Kazimierczuk, J. Sitkowski, J. Wietrzyk, E. Turlej, *J. Biol. Inorg. Chem.* **2019**, *24*, 591–606.
[22] J. Markham, J. Liang, A. Levina, R. Mak, B. Johannessen, P. Kappen, C. J. Glover, B. Lai, S. Vogt, P. A. Lay, *Eur. J. Inorg. Chem.* **2017**, *2017*, 1812–1823.
[23] W. Su, Z. Luo, S. Dong, X. Chen, J.-a. Xiao, B. Peng, P. Li, *Photodiagn. Photodyn. Ther.* **2019**, *26*, 448–454.
[24] T. Stringer, D. R. Melis, G. S. Smith, *Dalton Trans.* **2019**, *48*, 13143–13148.
[25] G. Gupta, P. Kumari, J. Y. Ryu, J. Lee, S. M. Mobin, C. Y. Lee, *Inorg. Chem.* **2019**, *58*, 8587–8595.
[26] W. D. J. Tremlett, K. K. H. Tong, T. R. Steel, S. Movassaghi, M. Hanif, S. M. F. Jamieson, T. Söhnel, C. G. Hartinger, *J. Inorg. Biochem.* **2019**, *199*, 110768.
[27] J. P. Mészáros, J. M. Poljarevic, G. T. Gál, N. V. May, G. Spengler, É. A. Enyedy, *J. Inorg. Biochem.* **2019**, *195*, 91–100.
[28] R. Pettinari, F. Marchetti, C. Di Nicola, C. Pettinari, *Eur. J. Inorg. Chem.* **2018**, *2018*, 3521–3536.
[29] Z. Liu, L. Salassa, A. Habtemariam, A. M. Pizarro, G. J. Clarkson, P. J. Sadler, *Inorg. Chem.* **2011**, *50*, 5777–5783.
[30] V. Novohradsky, Z. Liu, M. Vojtiskova, P. J. Sadler, V. Brabec, J. Kasparkova, *Metallomics* **2014**, *6*, 682–690.
[31] Z. Liu, I. Romero-Canelón, B. Qamar, J. M. Hearn, A. Habtemariam, N. P. E. Barry, A. M. Pizarro, G. J. Clarkson, P. J. Sadler, *Angew. Chem. Int. Ed.* **2014**, *53*, 3941–3946; *Angew. Chem.* **2014**, *126*, 4022.
[32] J. J. Soldevila-Barreda, A. Habtemariam, I. Romero-Canelón, P. J. Sadler, *J. Inorg. Biochem.* **2015**, *153*, 322–333.
[33] S. Banerjee, J. J. Soldevila-Barreda, J. A. Wolny, C. A. Wootton, A. Habtemariam, I. Romero-Canelón, F. Chen, G. J. Clarkson, I. Prokes, L. Song, P. B. O'Connor, V. Schünemann, P. J. Sadler, *Chem. Sci.* **2018**, *9*, 3177–3185.
[34] J. Tönnemann, J. Risse, Z. Grote, R. Scopelliti, K. Severin, *Eur. J. Inorg. Chem.* **2013**, *2013*, 4558–4562.
[35] L. Li, W. W. Brennessel, W. D. Jones, *J. Am. Chem. Soc.* **2008**, *130*, 12414–12419.
[36] S. Betanzos-Lara, Z. Liu, A. Habtemariam, A. M. Pizarro, B. Qamar, P. J. Sadler, *Angew. Chem. Int. Ed.* **2012**, *51*, 3897–3900; *Angew. Chem.* **2012**, *124*, 3963.
[37] Z. Liu, R. J. Deeth, J. S. Butler, A. Habtemariam, M. E. Newton, P. J. Sadler, *Angew. Chem. Int. Ed.* **2013**, *52*, 4194–4197; *Angew. Chem.* **2013**, *125*, 4288.
[38] Y. Hu, L. Li, A. P. Shaw, J. R. Norton, W. Sattler, Y. Rong, *Organometallics* **2012**, *31*, 5058–5064.
[39] Y. Hu, J. R. Norton, *J. Am. Chem. Soc.* **2014**, *136*, 5938–5948.
[40] Z. Liu, A. Habtemariam, A. M. Pizarro, G. J. Clarkson, P. J. Sadler, *Organometallics* **2011**, *30*, 4702–4710.
[41] D. E. Fisher, *Cell* **1994**, *78*, 539–542.
[42] O. V. Dolomanov, L. J. Bourhis, R. J. Gildea, J. A. Howard, H. Puschmann, *J. Appl. Crystallogr.* **2009**, *42*, 339–341.
[43] G. M. Sheldrick, *Acta Crystallogr., Sect. A* **2015**, *71*, 3–8.
[44] G. M. Sheldrick, *Acta Crystallogr., Sect. C* **2015**, *71*, 3–8.
[45] V. Vichai, K. Kirtikara, *Nat. Protoc.* **2006**, *1*, 1112–1116.

Received: October 5, 2019

Anticancer Complexes

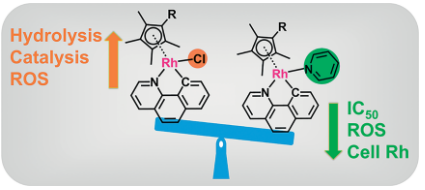

The chemical reactivity and cytotoxicity of half-sandwich organo-rhodium complexes can be controlled by the monodentate ligand. Chlorido complexes show faster hydrolysis and higher catalytic efficiency, but pyridine complexes exhibit higher cytotoxicity with lower cellular Rh accumulation. The pyridine complexes act as ROS scavengers, while the chlorido analogues elevate ROS levels in cancer cells.

DOI: 10.1002/ejic.201901055

